Journal of Materials Chemistry C

Accepted Manuscript

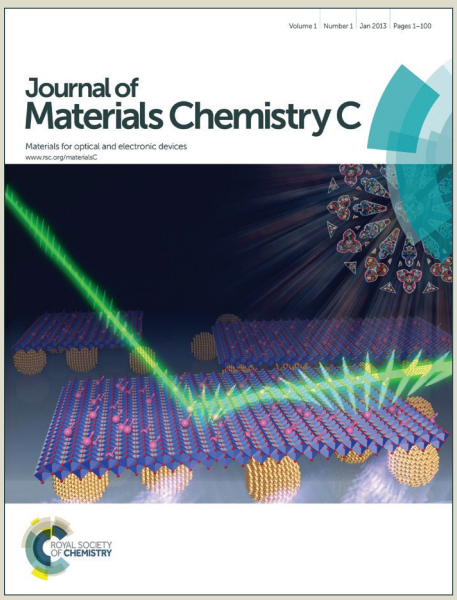

ROYAL SOCIETY OF CHEMISTRY

www.rsc.org/materialsC

ARTICLE TYPE www. rsc.org/xxxxxx | XXXXXXXX

Semi-metallic, Strong and Stretchable Wet-spun Conjugated Polymer Microfibers†

Jian Zhou,[‖a] Er Qiang Li,[‖b] Ruipeng Li,[c] Xuezhu Xu, [d] Isaac Aguilar Ventura,[a] Ali Moussawi,[a] Dalaver H. Anjum,[e] Mohamed Nejib Hedhili,[e] Detlef-M. Smilgies,[c] Gilles Lubineau *[a] and Sigurdur T. Thoroddsen *[b]

Received Xth XXXXXXXXXX 20XX, Accepted Xth XXXXXXXXX 20XX
First published on the web Xth XXXXXXXXXX 200X
DOI: 10.1039/b000000x

A dramatic improvement in electrical conductivity is necessary to make conductive polymer fibers viable candidates in applications such as flexible electrodes, conductive textiles, and fast-response sensors and actuators. In this study, high-performance poly(3,4-ethylenedioxythiophene)/poly(styrenesulfonate) (PEDOT/PSS) conjugated polymer microfibers were fabricated via wet-spinning followed by hot-drawing. Due to the combined effects of the vertical hot-drawing process and doping/de-doping the microfibers with ethylene glycol (EG), we achieved a record electrical conductivity of 2804 $S \cdot cm^{-1}$. This is, to the best of our knowledge, a six-fold improvement over the best previously reported value for PEDOT/PSS fibers (467 $S \cdot cm^{-1}$) and a two-fold improvement over the best values for conductive polymer films treated by EG de-doping (1418 $S \cdot cm^{-1}$). Moreover, we found that these highly conductive fibers experience a semiconductor-metal transition at 313 K. They also have superior mechanical properties with a Young's modulus up to 8.3 GPa, a tensile strength reaching 409.8 MPa and a large elongation before failure (21%). The most conductive fiber also demonstrates an extraordinary electrical performance during stretching/unstreching: the conductivity increased by 25% before the fiber rupture point with a maximum strain up to 21%. Simple fabrication of the semi-metallic, strong and stretchable wet-spun PEDOT/PSS microfibers described here could make them available for conductive smart electronics.

1 Introduction

Fiber-shaped conductive materials are attractive for use in applications ranging from simple textiles to complex multimaterial piezoelectric fibres and supercapacitors.[1–6] Conjugated polymer fibers, featuring tunable electrical conductivity, have been extensively investigated from both fundamental and application perspectives to understand their electrical and mechanical properties and their practical use in conducting textiles, organic electronics, sensors and actuators.[7–12] The main techniques for processing polymer fibers are dry-spinning, wet-spinning, melt-spinning and electrospinning.[13] In particular, wet-spinning is a relatively simple process to produce continuous polymer microfibers by submerging the spinneret in a coagulation bath that causes the fiber to solidify.[13,14]

Among the popular conjugated polymers, polypyrrole (PPy), polyaniline (PANI) and poly(3,4-ethylenedioxythiophene)/poly(styrenesulfonate)(PEDOT/PSS) have been successfully spun into microfibers by the wet-spinning process.[8,9,11,15] PEDOT/PSS has been found to have the best spinnability and its preparation technique can be scaled up to an industrial process.[16] In the past decade, doping and/or de-doping with various polar solvents has been carried out to enhance the conductivity of PEDOT/PSS films and fibers by two or three orders of magnitude.[9,17–21] Doping PEDOT/PSS involves mixing it with a small amount of secondary dopant (with a high boiling point and < 6 wt%) to change its microstructure to a more conductive state; de-doping requires partially removing amorphous PSS by washing it with polar solvents. Depending on grade of the employed pristine PEDOT/PSS, as-spun microfibers (without any doping) generally display low electrical conductivity (from 1 to 74 $S \cdot cm^{-1}$).[8,9] Their electrical conductivity could be improved up to 467 $S \cdot cm^{-1}$ by using an ethylene glycol (EG) de-doping process,

† Electronic Supplementary Information (ESI) available. See DOI: 10.1039/b000000x/

‖ Contributed equally to this work

[a] *King Abdullah University of Science and Technology (KAUST), Physical Sciences and Engineering Division, COHMAS Laboratory, Thuwal 23955-6900, Saudi Arabia; E-mail: gilles.lubineau@kaust.edu.sa; Tel:+966(12)8082983*
[b] *King Abdullah University of Science and Technology (KAUST), Physical Sciences and Engineering Division, High-Speed Fluids Imaging Laboratory, Thuwal 23955-6900, Saudi Arabia; E-mail: sigurdur.thoroddsen@kaust.edu.sa*
[c] *Cornell High Energy Synchrotron Source, Wilson Laboratory, Cornell University, Ithaca, New York 14853, USA.*
[d] *North Dakota State University, Department of Mechanical Engineering, Fargo, ND 58108, United States*
[e] *King Abdullah University of Science and Technology (KAUST), Advanced Nanofabrication, Imaging and Characterization Core Laboratory, Thuwal 23955-6900, Saudi Arabia*

which partially removes the amorphous and insulating PSS phase.[8] Jalili *et al.*[9] showed that by combining doping and de-doping, the electrical conductivity of PEDOT/PSS microfibers could reach 351 $S \cdot cm^{-1}$. Spinning PEDOT/PSS with functionalized carbon nanotubes into fibers led to limited improvement in conductivity (400 $S \cdot cm^{-1}$).[22,23] To meet the requirements for use as flexible electrodes, conductive textiles and fast-response sensors and actuators, such conductive polymer fibers must have dramatically improved electrical conductivity.

In this study, we fabricated semi-metallic, strong, and stretchable wet-spun PEDOT/PSS conjugated polymer microfibers. The novelty of our fabrication technique lies in a two-step method (wet-spinning followed by immediate hot-drawing) that greatly promotes molecular alignment. When combined with doping/de-doping by ethylene glycol (EG), it achieves a record electrical conductivity as high as 2804 $S \cdot cm^{-1}$. To the best of our knowledge, this is a six-fold improvement over the the best value previously reported for fibers (467 $S \cdot cm^{-1}$) and double the best value reported for PEDOT/PSS films treated with EG (1418 S cm^{-1}).[24] We found that these highly conductive fibers display a semiconductor-metal transition at 313 K. They also display superior mechanical properties: the Young's modulus is 8.3±0.4 GPa, the tensile strength is 409.8±13.6 MPa and the elongation at break for these fibers is 21.2±1.4%. These results show that the combined properties of the fibers have been remarkably improved in comparison with previously reported PEDOT/PSS fibers, as shown in Fig. 1a.

2 Experimental

2.1 Materials

The PEDOT/PSS aqueous dispersion (Clevios^{TM} P and PH1000) was purchased from HC Starck, Inc. Ethylene glycol (EG), Isotropyl alcohol (IPA), acetone were purchased from Sigma-Aldrich.

2.2 Preparation of highly spinable PEDOT/PSS inks

10 mL of water was evaporated from 20 mL of the PH1000 dispersion (11 mg mL^{-1}) at 50 °C to increase the viscosity of the ink. Then 0.3 g of EG was mixed into the concentrated PH1000 dispersion (22 mg mL^{-1}) by a magnetic stirrer for two hours to enhance the electrical conductivity.[17,25,36] Then it was homogenized at 20,000 rpm for 5 mins using a T18 homogenizer (IKA) and followed by 20 mins bath sonication using a Brason 8510 sonicator (250 W, Thomas Scientific) at room temperature. Finally, the dispersion was degassed in a vacuum oven at room temperature (21 °C) before wet-spinning.

2.3 Wet-spinning of PEDOT/PSS fibers

The spinning formulation was loaded into a 5 mL glass syringe and spun into a coagulation bath though a metal needle with an inner diameter from 100 to 220 μm. The flow rate of the ink was controlled between 2 to 50 μL min^{-1} by using a syringe pump. The fibers were collected vertically onto a 50 mm winding spool, which gives a line speed of 2 to 4 m min^{-1}. The air temperature along the path of the fiber was controlled to 90°C by two vertically located hot-plates (see Fig. 1b) and was monitored by a thermocouple. After wet-spinning, de-doping of the as-spun fibers was carried out by immersing them in a EG bath for 1 hour and the fibers were then dried in air at 160 °C for 1 hour. Herein, as-spun PEDOT/PSS fiber, EG/(PEDOT/PSS) fiber, (PEDOT/PSS)/EG fiber and EG/(PEDOT/PSS)/EG fiber represent pristine PEDOT/PSS fiber, 3 wt% EG doped PEDOT/PSS fiber, EG de-doped PEDOT/PSS fiber and EG de-doped 3 wt% EG doped PEDOT/PSS fiber, respectively.

2.4 Characterization

Electrical resistance of the fibers was measured by using an Agilent 1252B multimeter. The electrodes on the fiber were made by connecting a copper wire to the fiber surface with silver epoxy. The distance between two contacts was about 10 mm. The temperature-dependent DC electrical conductivity was measured by the two probe method in a temperature controllable chamber, in which highly pure N_2 was purged at a flow rate of 200 mL min^{-1} to protect the sample and measurement electronics from the humid air. The electrical conductivity measurements of the specimens were carried out in the temperature range from -150 to 220 °C with a heating rate of 5 °C min^{-1}. At least three measurements were conducted for each type of fiber.

Scanning electron microscopy (SEM) was performed using a Quanta 3D (FEI Company). TEM samples were prepared by focused ion beam (FIB) cutting with help from the same SEM machine. The conductive fibers were first fixed on the SEM holder with silver epoxy. The samples were tilted 52 ° and cuts were made along the fiber axis direction. The ion beam source was a field-emission FIB with a Pt ion emitter, an ion beam voltage of 30 kV and a beam current of 0.47 nA.

X-ray photoelectron spectroscopy (XPS) analysis were carried out with a Kratos Axis Ultra DLD spectrometer equipped with a monochromatic Al Kα X-ray source ($h\nu = 1486.6$ eV) operating at 150 W, a multichannel plate and delay line detector under a vacuum of 1×10^{-9} mbar. All spectra were recorded using an aperture slot of 300×700 μm. The survey and high-resolution spectra were collected at fixed analyzer pass energies of 160 eV and 20 eV, respectively. The XPS peaks were analyzed using a Shirley-type background and a nonlinear least-squares fitting of the experimental data based

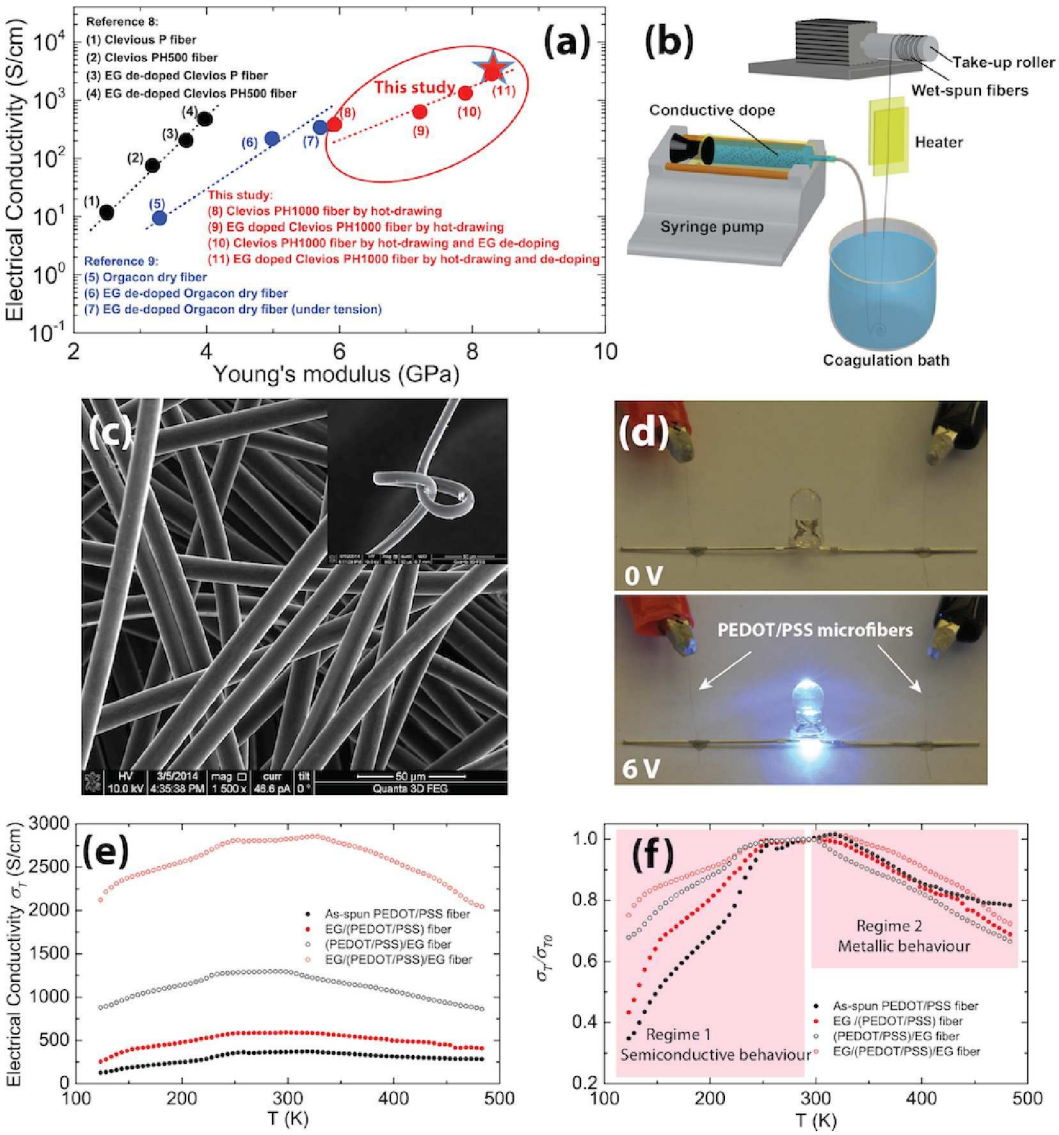

Fig. 1 Wet-spun PEDOT/PSS microfibers and their semi-metallic behaviors. (a) The electrical conductivity and Young's modulus of PEDOT/PSS microfibers. Black and blue dots denote reference values (ref 8 and 9), red dots denote values in this study. (b) A schematic of the wet-spinning set-up with the vertical hot-drawing apparatus used in this study. (c) SEM images of as-spun PEDOT/PSS fibers from a 22 mg/mL PH1000 dispersion. The inset is the SEM image of a knotted fiber. (d) Demonstration of a LED lit by two PEDOT/PSS fibers with diameters of 10 μm at 6 V. (e) Temperature-dependent electrical conductivity and (f) normalized electrical conductivity of an as-spun PEDOT/PSS fiber, an EG/(PEDOT/PSS) fiber, a (PEDOT/PSS)/EG fiber and an EG/(PEDOT/PSS/EG) fiber.

on a mixed Gauss/Lorentz peak shape. XPS quantification was performed by applying the appropriate relative sensitivity factors (RSFs) to the integrated peak areas.

Atomic Force Microscopy (AFM) images of conductive polymer fibers were taken using an Agilent 5400 (Agilent Technologies) microscope in the tapping mode over a window of 1 μm × 1 μm. The fibers were fixed on glass slides with a thin layer of epoxy adhesive.

TEM images of conductive polymer fibers were taken by using a Titan G2 80-300 CT (FEI Company) at an accelerating voltage of 300 kV equipped with a field-emission electron source. The PEDOT/PSS thin films cut from fibers by FIB were analyzed with High-Angle Annular Dark-field Scanning Transmission Electron Microscopy (HAADF-STEM) observation modes at a dose of 187 e Å^{-2}. The HAADF-STEM micrographs were recorded with an analog detector (E. A. Fis-

chione, Inc). The entire image acquisition as well as processing of the data was accomplished by using the GMS v1.8.3 microscopy suite software (Gatan, Inc).

Transmission Wide-angle X-ray Scattering (WAXS) measurements were performed on the D-line, Cornell High Energy Synchrotron Source (CHESS) at Cornell University. The fibers were aligned vertically into a bundle and placed perpendicularly into a monochromatic x-ray beam with the wavelength of 0.115 nm. The scattering patterns were collected by a CCD detector (Medoptics) with a pixel size of 46.9 μm at a distance 100 mm away from sample. The exposure time was 10 s. To present the anisotropic scattering, the plots were integrated along the horizontal and vertical directions in the $\pm 5^{\circ}$ region by the Fit2d program.[26]

Normal WAXD tests were performed from 2 to 35 $^{\circ}$ in a continuous mode using a Bruker D8 Advance powder X-ray diffractometer, with Cu-$K\alpha$ radiation (λ =1.54 Å) at 40 kV and 40 mA. To generate peaks with relatively high intensity, a slow increment at 0.02 $^{\circ}$ and a slow scan speed at 12 sec/step was applied. the percentage of crystallinity was determined by the Diffract.EVA software (Bruker). Raman spectra were collected using a LabRAM Aramis Raman spectrometer (Horiba, Ltd.) on casted films and fibers using a 632 nm laser.

The mechanical behavior of the fibers was measured by an 5966 Instron universal testing machine at a strain rate of 5% min^{-1}. The tests were performed inside an enclosure to protect the fibers from environmental disturbances. 2 cm long fibers were prepared and fixed on a paper card. The tensile strength, Young's modulus and elongation were calculated, and the values were collected from at least 10 tests for each formulation. The electrical resistance change of the fibers was monitored using an U1252B digital multimeter. A cyclic loading/unloading program was applied to the fiber with an incremental extension of 0.2 mm at each cycle and then releasing to a load of 1 mN. The resistance data were captured every 1 s during the test. Two ends of the samples were connected with copper wires and painted with silver epoxy, followed by sealing the silver epoxy area by an epoxy glue.

3 Results and discussion

3.1 The effect of hot-drawing on the conductivity of as-spun PEDOT/PSS fibers

Fig. 1b shows a schematic of the wet-spinning process (see the experimental section for details). A vertical hot-drawing system was set up to process the "wet" fibers as they are pulled out of the acetone/isopropyl alcohol (acetone/IPA) coagulation bath. Optimization of the wet-spinning parameters to achieve the highest reported conductivity of as-spun fibers is described in the Supporting Information. The vertical hot-drawing process helps to align the molecular chains of the fibers in the fiber direction. The draw ratio is calculated from the ratio of the fiber collection speed and the wet-spinning speed (see details in the supporting Information and Fig. S2†). Spinning of a pristine PH1000 dispersion (11 mg/mL) by using this system resulted in a discontinuous spinning process producing fibers with lengths up to 20 m at a draw ratio of 3.0. These fibers had an average diameter of 4.9$\pm$0.6 μm (Fig. S3a†). The spinnability of the fiber was dramatically improved by doubling the concentration of the PH1000 dispersion (22 mg/mL), resulting in fibers with lengths up to 100 m, while the diameter increased to 9.8$\pm$1.3 μm, as measured in SEM image (Fig. 1c). The fibers were found to have remarkably smooth surfaces and they could be easily knotted, demonstrating their excellent flexibility (inset of Fig. 1c). The electrical conductivity of the fibers spun from these two concentrations were 361$\pm$31 and 368$\pm$34 $S \cdot cm^{-1}$, respectively. These results suggest that the initial concentration of the dispersion does not affect the fiber conductivity by much. It is important to point out that no pretreatment was done on these dispersions and that the conductivity values were five times higher than the highest previous values of as-spun PEDOT/PSS fibers (74 $S \cdot cm^{-1}$)[8] and three orders of magnitude higher than that of bulk film (0.7 $S \cdot cm^{-1}$).[17] Fibers without hot-drawing (draw ratio = 1) from the concentrated dispersion (22 mg/mL) were also fabricated and had a diameters of 24.9$\pm$1.3 μm (Fig. S3b†). The conductivity of these fibers without hot-drawing was 188$\pm$16 $S \cdot cm^{-1}$, which was only half of the value of the hot-drawn fibers. To further confirm effect of the hot-drawing, another source of PEDOT/PSS dispersion (Clevios P, 13 mg/mL) was also spun into much thinner fibers with diameters of 2.9$\pm$0.2 μm using the hot-drawing process (Fig. S3c†). The conductivity of these Clevios P microfibers was 121$\pm$11 $S \cdot cm^{-1}$, which is one order of magnitude higher than that of the earlier reported value (11 $S \cdot cm^{-1}$ with a diameter of 4.5 μm).[8] These results suggest that hot-drawing process with a draw ratio of 3.0 serves to reduce fiber diameter and contribute to the increased conductivity observed. As a result, we attributed the improvement in the conductivity of the fibers to the preferential alignment of the molecular chains along the fiber axis induced by the hot-drawing. By using a simple hot-drawing assisted wet-spinning process, we could therefore fabricate fibers with electrical conductivity comparable with that of fibers doped and/or de-doped by organic solvent.

3.2 The effect of EG doping and/or de-doping

To obtain the highest possible electrical conductivity of the conjugated polymer fibers, doping and/or de-doping processes were applied to these fibers, as shown in Table S1† . First, doping was accomplished by adding 3 wt% EG with respect to the concentrated PH1000 dispersion (22 mg/mL). The aver-

age diameter of the fabricated fibers (EG/(PEDOT/PSS) fiber) was 9.7±1.4 μm (Fig. S3d†) and the conductivity readily improved from 368±34 to 607±60 $S \cdot cm^{-1}$. This conductivity enhancement was due to the microstructure arrangement of the PEDOT chains. The dipole-dipole interaction of EG with thiophene rings results in a planarization of the PEDOT chains. The quinoid structure becomes the dominating conformation on the chains. Thus, the PEDOT chains transformed from a coil to an expanded coil or linear structure after doping.[9]

The effect of de-doping was studied separately. Specifically, the as-spun fibers produced from the concentrated PH1000 dispersion (22 mg/mL) were de-doped by directly immersing the fibers in an EG bath for 1 hour and a conductivity of 1304±56 $S \cdot cm^{-1}$ was achieved. The main reason for the conductivity enhancement by de-doping is the partially removal of amorphous PSS.[8]

Earlier research has shown that an effective way of achieving the highest conductivity (1418 $S \cdot cm^{-1}$) of PEDOT/PSS films is to use both doping and de-doping processes together.[24]. Here, following the same idea and incorporating these processes with the hot-drawing process, we achieved a striking increase in the electrical conductivity of the fibers: from 607±60 $S \cdot cm^{-1}$ to 2804±311 $S \cdot cm^{-1}$. This value is six times better than best value for previous reported fibers (467 $S \cdot cm^{-1}$) and twice the best value (1418 $S \cdot cm^{-1}$) of PEDOT/PSS films with EG treatment.[24] Although a conductivity for PEDOT/PSS film ranging from 2400 to 4380 $S \cdot cm^{-1}$ has been achieved by treating the film with sulfuric acid, the use of strong and corrosive acid will cause safety concerns and is undesirable in commercial device fabrication.[18,27] In this work, simply by assisting the wet-spinning process with hot-drawing and doping/de-doping the fibers with EG, we can achieve a high conductivity that is comparable with the highest values for PEDOT/PSS films. We also demonstrate the electrical properties of our fibers by wiring a light-emitting diode (LED) with two PEDOT/PSS conductive fibers. The fiber resistance was low enough to light the LED at 6 V, as shown in Fig. 1d.

3.3 The Semi-metallic behavior of the fibers

Apart from the electrical conductivity at room temperature (RT), a second important factor characterizing electrical transport in conductive fibers is the dependence of conductivity on temperature. In previous study, we shown that pristine PEDOT/PSS film exhibits a typical semiconductor behavior with a positive temperature coefficient in the 123-523 K range.[28] However, the electrical behavior of PEDOT/PSS fibers is quite different than films. Fig. 1e shows the temperature-dependent conductivity of an as-spun PEDOT/PSS fiber, an EG/(PEDOT/PSS) fiber, a (PEDOT/PSS)/EG fiber and an EG/(PEDOT/PSS)/EG fiber. All these fibers exhibited two regimes in the conductivity: at low temperature, the conductivity rises with temperature (semiconductive behavior), whereas at high temperature, the conductivity drops (metallic behavior). The crossover temperature for the semiconductor-metal (S-M) transition is around 313 K (40 °C). The insulator-metal (I-M) or (S-M) transition in conductive polymers or carbon-based fibers has been observed in a wide temperature range in a number of systems, including polyacetylene, polypyrrole, polyaniline, polythiophene derivatives and carbon nanotubes.[3,29–34] Generally, the crossover temperature, T_0, of conductive polymers has been reported to be below room temperature, whereas T_0 of CNT fibers has been reported to vary from 40 K to well above room temperature.[3,34] The conductivity ratio, $\sigma(T)/\sigma(T_0)$, has been chosen to qualify the relative disorder in different samples and for identification of the various regimes.[29] Fig. 1f shows that the semiconductive behavior is more pronounced for low conductivity fibers. The typical semiconductive behavior that the fibers displayed at low temperature can be understood as carrier hopping or tunneling between adjacent PEDOT/PSS grains. These points will be addressed in detail in the following discussions. At high temperature, metallic behavior in EG doped and/or de-doped fibers indicates diffusive, intra-chain transport, during which the conductivity is reduced by electron-phonon scattering.

3.4 Microstructure characterization

To understand the electrical properties of the conductive fibers, we studied the surface and inner structural changes of the fibers. We used X-ray photoelectron spectroscopy (XPS) to investigate the as-spun PEDOT/PSS fibers and EG/(PEDOT/PSS) fibers before and after EG de-doping. High-resolution XPS of the S 2p core-level spectra are shown in Fig. 2a and b. The S 2p core-level has a signature with two distinct peaks from 162 to 166 eV and from 166 to 171 eV. Each peak involves contributions from a spin-split doublet, S $2p_{3/2}$ and S $2p_{1/2}$, with 1.2 eV energy splitting and a 1:2 intensity ratio.[35] The two peaks from 162 to 166 eV are well separated compared with the peaks from 166 to 171 eV. The S $2p_{3/2}$ components at 163.3 eV and 167.6 eV correspond to sulfur atoms of the PEDOT and the sulfonate fragment of PSS, respectively.[18,36,37] The experimental PEDOT-to-PSS ratio (R_s) was determined by quantitative analysis of the S 2p core-level spectra. In as-spun PEDOT/PSS fiber and EG/PEDOT/PSS fiber, the R_s are 0.50 and 0.52, respectively. By EG de-doping, the R_s increased to 0.86 and 1.04 for (PEDOT/PSS)/EG fiber and EG/(PEDOT/PSS)/EG fiber, respectively. This change clearly suggests that PSS are partially removed from fibers by EG de-doping. The fact that the EG/(PEDOT/PSS)/EG fiber also has the highest conductivity (2804 $S \cdot cm^{-1}$) also indicated that the less insulating polymer,

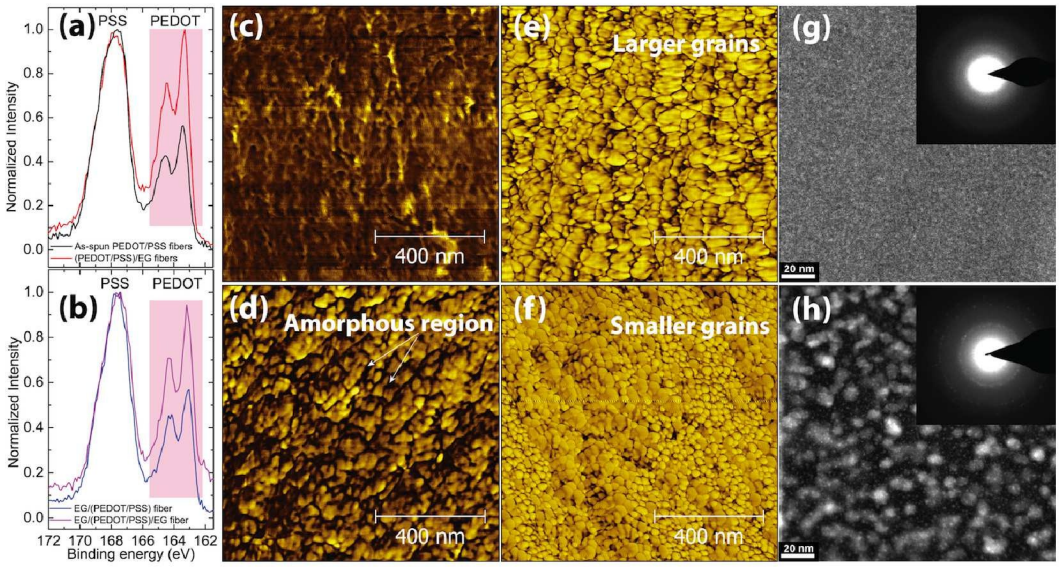

Fig. 2 Surface and inner structure characterizations of wet-spun PEDOT/PSS microfibers. (a) S 2p XPS spectra of as-spun PEDOT/PSS fibers before and after EG de-doping. (b) S 2p XPS spectra of EG doped PEDOT/PSS fibers before and after EG de-doping. The shaded area in shows the increased intensity of PEDOT after EG de-doping. (c), (d), (e) and (f) are AFM phase images of the as-spun PEDOT/PSS fiber, EG/(PEDOT/PSS) fiber, (PEDOT/PSS)/EG fiber and EG/(PEDOT/PSS/EG) fiber, respectively. (g) and (h) HADDAF-STEM images of the as-spun PEDOT/PSS fiber and EG/(PEDOT/PSS/EG) fiber, respectively. Selected area electron diffraction (SAED) patterns in the insets (g) and (h) indicate random-oriented polycrystalline and preferred-oriented polycrystalline, respectively.

PSS, in the fiber will increase the electrical conductivity.

AFM images were taken to probe the changes in the surface microstructures of all fibers. The root mean square (rms) roughnesses measured from height images of as-spun PEDOT/PSS fiber and EG/(PEDOT/PSS) fiber were 11.2 and 14.1 nm, respectively. After de-doping with EG, the roughnesses increased to 21.8 and 18.0 nm, respectively (Fig. S4†). This trend is in agreement with observations of PEDOT/PSS films with EG de-doping[17] and suggests partial removal of PSS segments in the fibers as indicated by XPS results. In the AFM phase images (Fig.s 2c and d), the EG/(PEDOT/PSS) fiber shows an obvious phase separation between PEDOT and PSS compared with the as-spun PEDOT/PSS fiber, indicating that EG doping can largely reduce electrostatic interactions between PEDOT and PSS.[38] The dark areas can be regarded as the amorphous PSS region, while the bright areas are the conductive PEDOT region. As the thick and insulating PSS acts as barriers for electron transport between PEDOT grains, the conductivity of these fibers is relatively low. Fig. 2e and f show that after EG de-doping, the amorphous regions (PSS) of both fibers are largely reduced, resulting in interconnected PEDOT grains with an extremely thin layer of PSS between them. The average size of the grains in the EG/(PEDOT/PSS)/EG fiber (14.8 ±4.4 nm) is much smaller than that in the (PEDOT/PSS)/EG fiber (56.8 ±12.7 nm). The reduction of grain size indicates that more PSS is removed from the EG/(PEDOT/PSS) fibers after de-doping. This change is also in agreement with the increased R_s (0.86 and 1.04 for the (PEDOT/PSS)/EG fiber and EG/(PEDOT/PSS)/EG fiber, respectively). A crucial point is that doping PEDOT/PSS makes the de-doping step more efficient by reorganising the initial microstructure of the fiber. As there is a very limited amount of PSS between the conductive PEDOT grains, this leads to an increased number of interconnections with highly conductive PEDOT neighbor grains on the surface of the fibers and makes the electron transport easier, thereby resulting in the highest conductivity of the fibers considered in this study.

To investigate the inner microstructural changes between the as-spun PEDOT/PSS fiber and the EG/(PEDOT/PSS)/EG fiber, the samples were cut into nanofilms by Focused Ion Beam (FIB) along the fiber axis direction and investigated by High-Angle Annular Dark-Field Scanning Transmission Electron Microscopy (HAADF-STEM). The average thickness of the films was determined to be 56.7 nm from the effective mean free path.[39] Fig. 2g shows that the as-spun PEDOT/PSS fiber exhibits no obvious grain structures compared with previous spin-coated PEDOT/PSS nanofilms[40], indicating that PEDOT/PSS has a very condensed fiber structure. With EG doping/de-doping, PEDOT/PSS aggregates with diameters of 8.5 ± 1.7 nm appear in the film (Fig. 2h). Small grains with a size down to 1 nm are also observed between these aggregates,

revealing that EG doping/de-doping releases conductive PEDOT from the PEDOT/PSS complex. The selected area electron diffraction (SAED) pattern of the as-spun PEDOT/PSS fibers shows amorphous rings, indicating that the crystallinity of PEDOT is inhibited by a strong electrostatic interaction with the entangled PSS. On the other hand, the SAED pattern of the EG/(PEDOT/PSS)/EG fiber is similar to PEDOT microribbons with a width of 1.8 μm[41], showing discrete diffraction spots in each Debye ring. These results suggest that after EG doping/de-doping, the PEDOT structure is rearranged from random-oriented polycrystalline to a preferred-oriented polycrystalline. Thus, interchain charge carrier transport will be significantly improved by the chain alignment so that the EG/(PEDOT/PSS)/EG fiber has the highest conductivity.

To understand the electrical transport in the fibers, the fiber microstructure was investigated by transmission Wide Angle X-ray Scattering (WAXS). The fibers are bundled and aligned perpendicularly to scatter the x-ray beam, as shown in Fig. S5† . Fig. 3 presents the 2D WAXS pattern and the intensity integration plots along the vertical and horizontal directions, presenting the anisotropic structure in the fibers. For the as-spun PEDOT/PSS fibers, three broad peaks are observed in the vertical direction at approximately q_z = 2.5, 11.6 and 17.5 nm^{-1}, corresponding to the d-spacing of 2.51, 0.541 and 0.359 nm (Fig. 3e), respectively. The (100) peak at q_z = 2.5 nm^{-1} is assigned to lamella stacking of alternate orderings of PEDOT and PSS in the plane. The (020) peak at q_z = 17.5 nm^{-1} indicates $\pi-\pi$ stacking of PEDOT chains along the vertical direction.[8,38]. The broad peak at q_z = 11.6 nm^{-1} is attributed to the amorphous halo of randomly distributed PSS.[27,38,42] On the other hand, the integrated plot in the horizontal direction, which shows the microstructure in the transverse fiber direction, has only a PSS peak but no (100) and (020) peaks (Fig. 3f). Due to the amorphous nature of PSS, there is no obvious anisotropy with this broad peak (q_{xy} = 11.6 nm^{-1}) in both directions. To conclude, the strong scattering anisotropy of PEDOT in as-spun PEDOT/PSS fibers reveals that the PEDOT chains orient preferentially along the fiber direction.

The EG doped fibers have a similar structure as the as-spun fibers but they have better crystallinity. Fig. 3c presents the WAXS pattern of EG/(PEDOT/PSS) fibers showing the higher intensity from both $\pi-\pi$ stacking and polymer backbones. The fibers made with 3 wt% EG-doped PEDOT/PSS exhibit narrower peaks at both q_z = 2.34 and 17.6 nm^{-1}, indicating that better crystallinity formed in the fibers. The broad hump peak at q_z = 11.6 nm^{-1} is more obvious, suggesting that EG weakens the electrostatic interactions between PSS and PEDOT. This improvement is consistent with observations in former AFM phase images (Fig. 2a,b), in which the phase segregation of PEDOT and PSS is more obvious than that of as-spun PEDOT/PSS fibers. It is worth noting that after de-doping, the $\pi-\pi$ stacking peak of as-spun PEDOT/PSS fibers and EG/(PEDOT/PSS) fibers shifted from q_z = 17.5 and 17.6 nm^{-1} to q_z = 17.9 and 18.0 nm^{-1}, respectively. The above peak shifts correspond to a reduction in the $\pi-\pi$ stacking distances from 3.59 and 3.57 to 3.51 and 3.48 Å, respectively. The shorter distance indicates stronger $\pi-\pi$ interactions between adjacent PEDOT chains, facilitating electron transport in these directions. There is also an obvious intensity reduction on the broad hump peak at q_z and q_{xy} =11.6 nm^{-1}, as manifested by the partial removal of PSS in XPS results (Fig. 2a,b). The alignment of molecule along the fiber axis is determined by Herman's orientation factor (f)[43]:

$$f = \frac{3(\cos^2\theta)-1}{2} \quad (1)$$

where θ is the angle between the orienting entity and the fiber axis. The optimised alignment of the molecule chains was confirmed by observing Herman's orientation factor, 0.697 and 0.726 for as-spun PEDOT/PSS fiber and EG/(PEDOT/PSS)/EG fiber, respectively. Normal WAXS (Fig. S6a,b† , Fig. S7a† and Table S2†) were also performed and the results are comparable with those of transmission WAXS. We verified again that the most effective way to improve the order of the molecular chains and the crystalinity of the fibers involves stretching the molecular chains by hot-drawing, reducing of the PEDOT and PSS electrostatic interaction by EG doping and reducing the $\pi-\pi$ stacking distance of PEDOT chains by EG de-doping.

3.5 Mechanical and electromechanical behaviors

A most obvious feature of these fibers is that they can be easily shaped into highly flexible structures, which is crucial to successful applications requiring stretchable electronics and functional fabrics. To illustrate this, a bundle of fibers was wound around a thin glass capillary (diameter: 5 mm) to form a helical shape after drying (Fig. 4a). The spring-like bundle was then manually stretched from 3.5 cm to a final length of 12.5 cm, corresponding to an elongation of 257%. The stretched bundle did not break and could recover its original shape upon release.

Next, we investigated the single fiber mechanical behavior. Fig. 4b shows stress-strain curves obtained for fibers subjected to hot-drawing but with various formulations. All fibers display a bi-linear stress-strain curve, which is characteristic of linear strain-hardening behavior. The mechanical properties of these fibers are greatly improved over those of earlier reported PEDOT/PSS fibers.[7–9] First of all, we note that hot-drawing by itself already largely enhances the properties of the fibers. Indeed, as-spun PEDOT/PSS fibers have a tensile strength of 242.5 $\pm$ 21.0 MPa and a Young's modulus of 5.9 $\pm$ 0.7 GPa, which are already twice the values of as-spun fibers prepared from IPA coagulant in a previous study.[9] Further

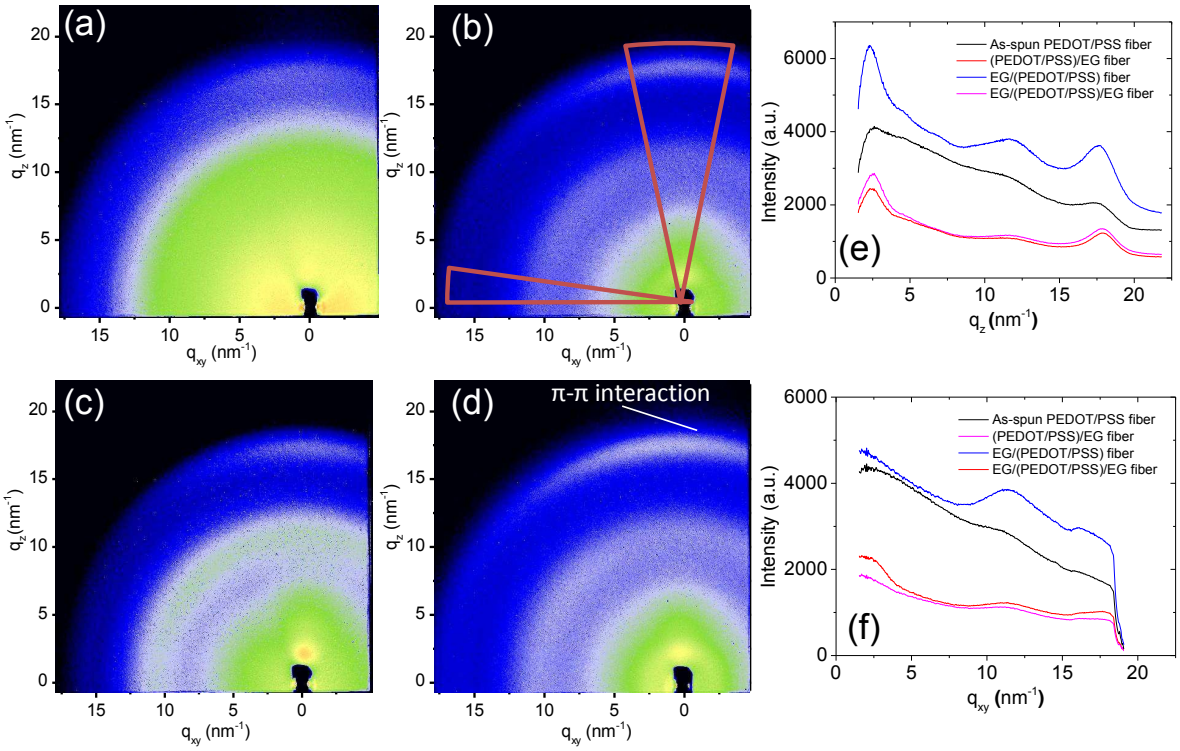

Fig. 3 Transmission WAXS characterization of PEDOT/PSS microfibers. 2D WAXS pattern of (a) as-spun PEDOT/PSS fibers, (b) (PEDOT/PSS)/EG fibers, (c) EG/(PEDOT/PSS) fibers and (d) EG/(PEDOT/PSS)/EG fibers. The red markers in (b) show the directions of intensity integration. (e) and (f) Intensity integration in the vertical and horizontal directions of all fibers.

SEM observation of the cross section of a broken fiber after mechanical testing did not reveal any obvious pores. More importantly, fibrilization at the fracture cross-section was observed (Fig. S8†), suggesting typical plastic deformation of the fibers.

Our results indicate that doping and/or de-doping the fibers with EG improved the mechanical properties. These fibers had a tensile strength of 409.8 ± 13.6 MPa and a Young's modulus of 8.3 ± 0.4 GPa, which are three and 1.5 times higher than previously reported, respectively.[9] Generally, we attribute these improvements to the partial removal of amorphous PSS (Fig. 2a,b) and an increase in the crystallinity of PEDOT/PSS fibers as shown in Fig. 3. Along with the increase in the Young's modulus, we observe that the plastic behavior was largely reduced after doping and de-doping. First, the yield stress, σ_y, increased from 135 MPa for the as-spun fibers to 187 MPa for the EG/(PEDOT/PSS)/EG fibers, indicating that the plasticity developed at a 38% higher load in the lastest. When plasticity was initiated ($> \sigma_y$), it also developed more slowly in the EG/(PEDOT/PSS)/EG fibers compared with the as-spun fibers. Indeed, this typical bi-linear behavior can be matched as a first approximation by a simple Prandtl-Reuss elasto-plastic model.[44] In this model, the classical linear hardening parameter, H, ranges from 0 for materials with perfect plasticity to $+\infty$ for perfectly elastic behaviors and it can be expressed as:

$$H = \frac{\sigma_m - \sigma_y}{D} \quad (2)$$

where σ_m is the final tensile stress and D is the plastic strain, as shown in Fig. 4a. H takes here the values 819, 1039, 1216 and 1315 MPa for the as-spun fibers, the EG/(PEDOT/PSS) fibers, the (PEDOT/PSS)/EG) fibers and the EG/(PEDOT/PSS)/EG fibers, respectively. The increases in the Young's modulus (E), the yield stress (σ_y) and the linear hardening parameter (H) are consistent with removal of the PSS phase. Indeed, the PEDOT/PSS fiber is in fact a composite between a soft and plastic phase (PSS) with a much stiffer and less plastic phase (PEDOT). Removal of PSS tends to increase the elastic properties while decreasing the plastic properties. Note that the mechanical tests in this work were performed at room temperature and 60% relative humidity (RH). It is expected that the values reported here for tensile strength and Young's modulus would further increase by reducing the RH level.[45,46] We also found that the fibers that display the highest modulus combined with the highest ultimate tensile strength (i.e., EG/(PEDOT/PSS)/EG fibers), are also those that exhibit the

highest electrical conductivity. Thus, the mechanical properties and electrical conductivity are improved in a correlated manner as the degree of chain alignment is increased, as shown in Fig. 1a.

The superior mechanical and electrical properties motivated us to further investigate the degradation of the mechanical and electrical properties by stretching/unstretching. First, we performed cyclic loading/unloading tests (Fig. 4c). These are consistent with the monotonic loading test in the sense that the former confirms the envelope of the cyclic curve, excluding any effect of the cycling on the envelope curve. To track any development of degradation within the fibers while increasing the loading, we followed a classical damage mechanics approach.[47] These materials display an elastic recovery due to the elastic and reversible part of the extension. It is important to note that the macroscopic elastic behaviour results from the superposition of both the amorphous elastic behavior and the crystalline elastic behavior (much stiffer). Therefore, the transition from a low modulus elastic phase to a high modulus elastic phase denotes an increase in the relative content of crystalline phase. The relative Young's modulus change, E_i/E_0, of as-spun PEDOT/PSS fibers and EG/(PEDOT/PSS)/EG fibers is plotted as a function of the maximum strain at each cycle (Fig. S9†), where E_0 and E_i are the initial and current Young's modulus, respectively. For the as-spun PEDOT/PSS fibers, we observe a 20% decrease in the Young's modulus at low strain levels ($< 4\%$). Beyond this point, the modulus increases slightly. This behavior in the low strain regime is attributed to the large amount of amorphous PSS in PEDOT/PSS fibers. At larger strains ($> 4\%$), the PEDOT crystalline region rotates the chain molecules into the fiber loading direction and the modulus increases again. In contrast, the Young's modulus of EG/(PEDOT/PSS)/EG fiber remains almost constant until the strain level increases over 4%. This can be explained by the fact of that partial removal of PSS can lead to an earlier rotation of the PEDOT crystalline region in comparison with the as-spun PEDOT/PSS fiber.

The relative resistance change ($\Delta R/R_0$) was also monitored under cyclic loading/unloading with progressive extension of the as-spun PEDOT/PSS fiber and EG/(PEDOT/PSS)/EG fiber (Fig. 4d,e). As expected, the resistance of the sample increases with increasing strain. The resistance in a bulk material with a circular cross section is given by:

$$R = \frac{l}{\pi r^2 \sigma}, \tag{3}$$

where σ is the electrical conductivity, and l and r are the length and the radius of the fiber, respectively. To determine the intrinsic conductivity change, the pure geometric factor was calculated and subtracted from the measured resistance. The relationship between the relative resistance change and the conductivity change can be expressed by:

$$\frac{\Delta R}{R_0} = -\frac{\Delta \sigma}{\sigma} + \frac{\Delta l}{l} - 2\frac{\Delta r}{r}. \tag{4}$$

For small changes $\Delta l/l = \varepsilon_l$ and $\Delta r/r = -\nu\varepsilon_l$, where ε_l is the strain in the fiber direction, and ν is the Poisson's ratio. substituting these values in equation (3) gives

$$\frac{\Delta R}{R_0} = -\frac{\Delta \sigma}{\sigma} + \varepsilon_l(1+2\nu), \tag{5}$$

where $F = \varepsilon_l(1+2\nu)$ comes only from the change in the cross-section of the fibers, whereas the first part on the right-side term, $\Delta\sigma/\sigma$, reflects changes in the conductivity of the material that can also be dependent on the strain.

For the as-spun PEDOT/PSS fibers, the relative resistance change is 0.23 at 13% strain level. Assuming $\nu = 0.34$[48], we can calculate F= 0.22 and $\Delta\sigma/\sigma \approx 0$. Therefore, the variation in resistance can be mostly attributed to the change in the geometry of the sample. However, it is important to highlight that the EG/(PEDOT/PSS)/EG fiber exhibits a much lower variation in resistance. At the same strain level of 13%, the resistance change is only 0.05, which is almost 3.5 times lower than that of the as-spun fiber. With the previous values, we find that $\Delta\sigma/\sigma = 0.17$, suggesting an increase in the conductivity of the fiber.

3.6 Correlation between the microstructure and the electrical and mechanical properties

The morphology, microstructure investigated by AFM and TEM together with the electromechanical analyses of the fibers provide some insight into the correlation between the PEDOT/PSS microstructure and the electrical and mechanical behaviors. The stages of the molecular level deformation of PEDOT/PSS fiber are proposed in Fig. 5a. PEDOT/PSS is a semi-crystalline complex, in which PEDOT is a conductive nanocrystal and PSS is an amorphous insulator.[38] The plastic deformation starts by lengthening amorphous PSS chains. At larger strains, the PEDOT crystalline region rotates the molecule chains into the fiber's loading direction. Further deformation results in crystalline regions separating into different blocks and amorphous regions form new layers among these blocks in the vertical direction. This rearrangement improves the dispersion of PEDOT nanocrystals in the fiber and the molecule chains tend to align with respect to the loading direction. Moreover, due to the low content of amorphous phase in the doped/de-doped material (EG/(PEDOT/PSS)/EG fiber), amorphous chains between crystalline islands are relatively short. Then, they can be easily stretched and tightened during the loading so finally the modulus increases as the amorphous chains become quickly straight. As the weakest part is the interface between amorphous and crystalline re-

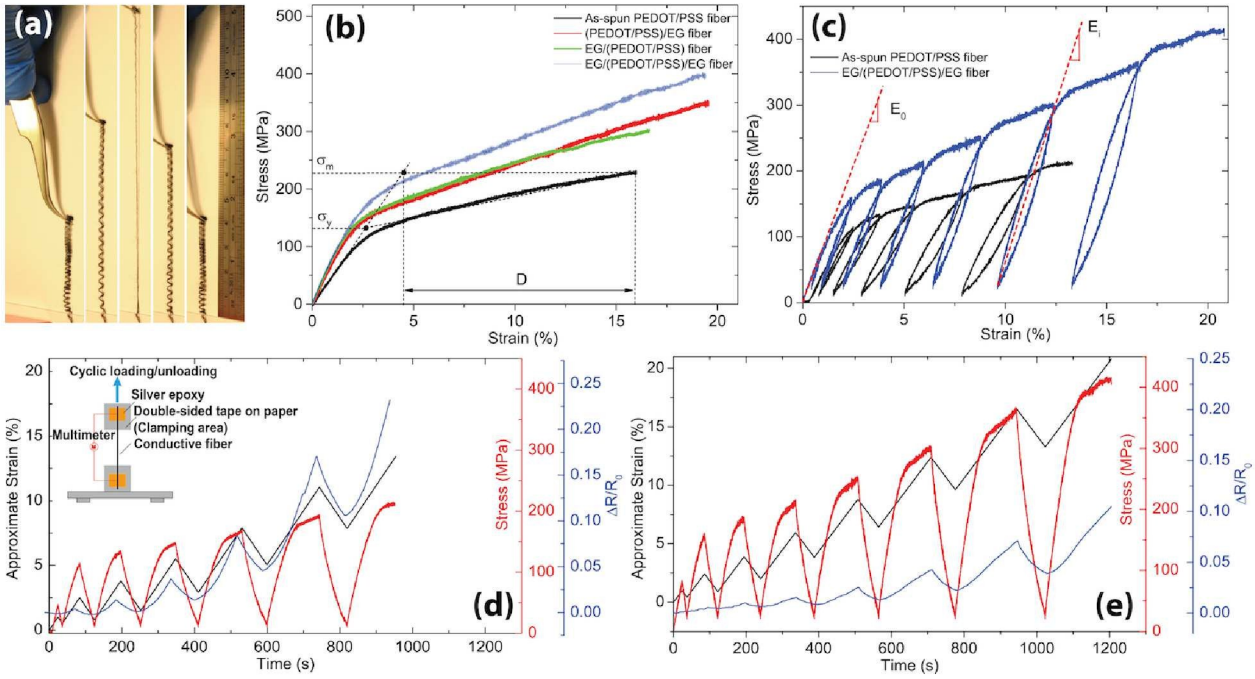

Fig. 4 The mechanical behaviors and electrical resistance changes in conjugated polymer fibers upon stretching/unstreching. (a) Strechability of a fiber bundle. The bundle was made into a spiral shape. The bundle can be stretched under a large strain and can recover almost to its original shape. (b) Representative stress-strain curves of the fibers. (c) Cyclic mechanical tests of as-spun PEDOT/PSS fibers and EG/(PEDOT/PSS)/EG fibers. (d), (e) The resistance change to the cyclic loading of as-spun PEDOT/PSS fibers and EG/(PEDOT/PSS)/EG fibers, respectively. The insert in (d) is a schematic of the response measurement sensor for the fibers.

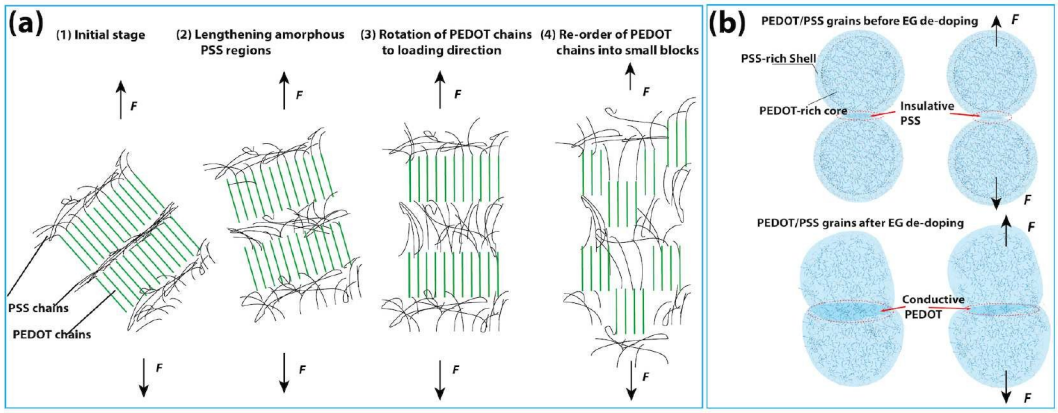

Fig. 5 Correlation between the PEDOT/PSS microstructure and electrical and mechanical properties. (a) Different stages of the molecular level deformation in a PEDOT/PSS fiber upon loading. (b) The grain-level deformation and resistance change mechanism of fibers before and after EG de-doping.

gions in PEDOT/PSS, deformation at the last stage may result in damage to the interfaces and rupture of the fiber.[49]

To address the mechanism that leads to electrical conductivity changes in the fibers, a schematic deformation of PEDOT/PSS grains in fibers before and after EG de-doping is displayed in Fig. 5b. A key point is that as-spun PEDOT/PSS fibers contain large amounts of amorphous PSS as insulators. Upon stretching, the PSS-rich shell around the PEDOT-rich core is elongated, so that the electron hopping distance between neighbor PEDOT/PSS grains in the fiber direction increases. This change obviously results in a larger $\Delta R/R_0$. In EG/(PEDOT/PSS)/EG fibers, the PSS insulator is partially

removed by EG de-doping, reducing the distance between PEDOT-rich cores and thereby creating conductive path ways. As a result, the $\Delta R/R_0$ for EG/(PEDOT/PSS)/EG fiber is dramatically reduced compared with that of as-spun PEDOT/PSS fibers under the same strain. Oh *et al.*[50] have shown that using PEDOT/PSS in electrodes and electrical circuits presents a number of challenges, especially that the conductivity decreases at large strains ($>$ **2%**). However, our conductive fibers show an extraordinary electrical performance during stretching/unstreching: the conductivity increased by 25% (as calculated from Equation (5)) before the fiber rupture point with the maximum strain up to 21%.

4 Conclusions

In conclusion, we systematically studied the effects of hot-drawing and EG doping/de-doping on the conductivity of wet-spun PEDOT/PSS microfibers. We achieved an extremely high values of bulk conductivity over 2800 $S \cdot cm^{-1}$. This conductivity value is comparable to the values of acid-treated PEDOT/PSS film (2400-4380 $S \cdot cm^{-1}$). The results also show a clear correlation between the microstructure and the electrical and mechanical properties. In particular, we found a maximum Young's modulus of 8.3 GPa for the most conductive fiber, which corresponds an increase of 41% over as-spun PEDOT/PSS fibers. The enhanced properties resulted from microstructural refinement, which was achieved by (1) preferred alignment of PEDOT molecule chains through hot-drawing, (2) reduction in the electrostatic interaction of PEDOT and PSS by EG doping and (3) partial removal of amorphous PSS from the fibers by EG de-doping. The fibers with enhanced properties also show superior stretchability and are able to retain high stiffness with an obvious increase in electrical conductivity (25%) at strain levels as high as 21%. These results may provide a foundation for performance maximization of conjugated polymer microfibers and our findings indicate the fibers has a high potential to be used in textile-based stretchable devices. For example, these light-weight, stretchable conductive polymer fibers could be applied more favorably than metallic wires with similar diameters in heating textiles, in which metallic wires are known to have poor flexibility, stretchability and poor tolerance to frequent bending and contact. Work is undergoing to apply these conductive polymer fibers as heating elements in smart textiles.

5 Acknowledgments

We thank Jun Li, Qingxiao Wang for their help with TEM sample preparation and Long Chen for taking AFM images. Research reported in this publication was supported by King Abdullah University of Science and Technology (KAUST). E. Q. L is grateful for a SABIC Postdoctoral Fellowship. CHESS is supported by NSF and NIH/NIGMS via NSF award DMR-1332208.

References

1 K. Cherenack, C. Zysset, T. Kinkeldei, N. Munzenrieder and G. Troster, *Adv. Mater.*, 2010, **22**, 5178.
2 A. F. Abouraddy, M. Bayindir, G. Benoit, S. D. Hart, K. Kuriki, N. Orf, O. Shapira, F. Sorin, B. Temelkuran and Y. Fink, *Nat. Mater.*, 2007, **6**, 336–347.
3 N. Behabtu, C. C. Young, D. E. Tsentalovich, O. Kleinerman, X. Wang, A. W. K. Ma, E. A. Bengio, R. F. ter Waarbeek, J. J. de Jong, R. E. Hoogerwerf, S. B. Fairchild, J. B. Ferguson, B. Maruyama, J. Kono, Y. Talmon, Y. Cohen, M. J. Otto and M. Pasquali, *Science*, 2013, **339**, 182–186.
4 S. Egusa, Z. Wang, N. Chocat, Z. M. Ruff, A. M. Stolyarov, D. Shemuly, F. Sorin, P. T. Rakich, J. D. Joannopoulos and Y. Fink, *Nat. Mater.*, 2010, **9**, 643–648.
5 L. Kou, T. Huang, B. Zheng, Y. Han, X. Zhao, K. Gopalsamy, H. Sun and C. Gao, *Nat. Commun.*, 2014, DOI: 10.1038/ncomms4754.
6 Z. B. Yang, J. Deng, X. L. Chen, J. Ren and H. S. Peng, *Angew. Chem. Int. Ed. Engl.*, 2013, **52**, 13453–13457.
7 H. Okuzaki and M. Ishihara, *Macromol. Rapid. Commun.*, 2003, **24**, 261–264.
8 H. Okuzaki, Y. Harashina and H. Yan, *Europ. Polym. J.*, 2009, **45**, 256–261.
9 R. Jalili, J. M. Razal, P. C. Innis and G. G. Wallace, *Adv. Funct. Mat.*, 2011, **21**, 3363–3370.
10 J. Fanous, M. Schweizer, D. Schawaller and M. R. Buchmeiser, *Macromol. Mater. Eng.*, 2012, **297**, 123–127.
11 J. Foroughi, G. M. Spinks and G. G. Wallace, *J. Mater. Chem.*, 2011, **21**, 6421–6426.
12 C. Plesse, F. Vidal, D. Teyssie and C. Chevrot, *Chem. Commun.*, 2010, **46**, 2910–2912.
13 H. Jiang, W. Adams and R. Eby, in *High Performance Polymer Fibers*, WILEY-VCH, 1st edn, 2006, pp. 597–652.
14 X. Z. Xu, A. J. Uddin, K. Aoki, Y. Gotoh, T. Saito and M. Yumura, *Carbon*, 2010, **48**, 1977–1984.
15 S. J. Pomfret, P. N. Adams, N. P. Comfort and A. P. Monkman, *Polymer*, 2000, **41**, 2265–2269.
16 H. Miura, Y. Fukuyama, T. Sunda, B. Lin, J. Zhou, J. Takizawa, A. Ohmori and M. Kimura, *Adv. Eng. Mater.*, 2014, **16**, 550–555.
17 J. Zhou and G. Lubineau, *ACS. Appl. Mater. Interfaces.*, 2013, **5**, 6189–6200.
18 Y. Xia, K. Sun and J. Ouyang, *Adv. Mater.*, 2012, **24**, 2436–2440.

19 J. Ouyang, Q. Xu, C. Chu, Y. Yang, G. Li and J. Shinar, *Polymer*, 2004, **45**, 8443–8450.

20 B. H. Fan, X. G. Mei and J. Y. Ouyang, *Macromolecules*, 2008, **41**, 5971–5973.

21 Y. Xia and J. Ouyang, *ACS. Appl. Mater. Interfaces.*, 2012, **4**, 4131–4140.

22 R. Jalili, J. M. Razal and G. G. Wallace, *J. Mater. Chem.*, 2012, **22**, 25174–25182.

23 R. Jalili, J. M. Razal and G. G. Wallace, *Sci. Rep.*, 2013, **3**, 1–7.

24 Y. H. Kim, C. Sachse, M. L. Machala, C. May, L. Muller-Meskamp and K. Leo, *Adv. Funct. Mater.*, 2011, **21**, 1076–1081.

25 J. Zhou, I. Ventura and G. Lubineau, *Ind. Eng. Chem. Res.*, 2014, **53**, 3539–3549.

26 A. P. Hammersley, in *Mechanical behaviour of polymers*, 1998.

27 N. Kim, S. Kee, S. Lee, B. Lee, Y. Kahng, , Y. Jo, B. Kim and K. Lee, *Adv. Mater.*, 2014, **26**, 2268–2272.

28 J. Zhou, D. H. Anjum, Chen, X. Xu, I. Ventura, L. Jiang and G. Lubineau, *J. Mater. Chem. C*, 2014, **2**, 9903–9910.

29 A. Heeger, N. Sariciftci and E. Namdas, in *Metallic State of Conducting Polymers*, Oxford University Press, Oxford, New York, 1st edn, 2010, pp. 1–278.

30 B. Wessling, in *Conductive polymers as organic nanometals*, ed. T. Skotheim and J. Reynolds, CRC press, Boca Raton, London and New York, 3rd edn, 2007, vol. 2, pp. 1049–1122.

31 A. Epstein, in *InsulatorMetal Transition and Metallic State in Conducting Polymers*, ed. T. Skotheim and J. Reynolds, CRC press, Boca Raton, London and New York, 3rd edn, 2007, vol. 1, pp. 595–667.

32 K. Lee, S. Cho, S. H. Park, A. J. Heeger, C. W. Lee and S. H. Lee, *Nature*, 2006, **441**, 65–68.

33 A. S. Dhoot, J. D. Yuen, M. Heeney, I. McCulloch, D. Moses and A. J. Heeger, *Proc. Natl. Acad. Sci.*, 2006, **103**, 11834–11837.

34 A. Lekawa-Raus, J. Patmore, L. Kurzepa, J. Bulmer and K. Koziol, *Adv. Funct. Mater.*, 2014, **24**, 3661–3682.

35 A. Schaarschmidt, A. Farah, A. Aby and H. AS, *J. Phys. Chem. B.*, 2009, **113**, 9352–9355.

36 G. Kim, L. Shao, K. Zhang and K. Pipe, *Nat. Mater.*, 2013, **12**, 719–723.

37 Z. Vardeny and O. Korovyanko, in *Photoelectron Spectroscopy of Conjugated Polymers*, ed. T. Skotheim and J. Reynolds, CRC press, Boca Raton, London and New York, 3rd edn, 2007, vol. 1, pp. 907–940.

38 T. Takano, H. Masunaga, A. Fujiwara, H. Okuzaki and T. Sasaki, *Macromolecules*, 2012, **45**, 3859–3865.

39 D. Williams and C. Carter, in *D. Williams and C. Carter*, Springer, Boca Raton, London and New York, 2nd edn, 2009, pp. 79–100.

40 U. Lang, E. Müller, N. Naujoks and J. Dual, *Adv. Funct. Mater.*, 2009, **19**, 1215–1220.

41 B. Cho, K. Park, J. Baek, H. Oh, L. YK and M. Sung, *Nano Lett*, 2014, **14**, 3321–3327.

42 N. Kim, B. H. Lee, D. Choi, G. Kim, H. Kim, J. R. Kim, J. Lee, Y. H. Kahng and K. Lee, *Phys. Rev. Lett.*, 2012, **109**, year.

43 A. Bhattacharyya, T. V. Sreekumar, T. Liu, S. Kumar, L. Ericson, R. Hauge and R. Smalley, *Polymer*, 2003, **44**, 2373–2377.

44 P. Ladevèze and J. Pelle, *Mastering Calculations in Linear and Nonlinear Mechanics*, Springer New York, 1986.

45 H. Okuzaki, H. Suzuki and T. Ito, *J. Phys. Chem. B.*, 2009, **113**, 11378–11383.

46 J. Zhou, T. Fukawa, H. Shirai and M. Kimura, *Macromolecular. Mater. Eng.*, 2010, **295**, 671–675.

47 L. Kachanov, *Introduction to Continuum Damage Mechanics*, Springer Science and Business Media, 2nd edn, 1986.

48 U. Lang, N. Naujoks and J. Dual, *Synth. Met.*, 2009, **159**, 473–479.

49 J. Roesler, H. Harders and M. Baeker, in *Mechanical Behaviour of Polymers*, Springer, Berlin, Heidelberg and New York, 1st edn, 2007, pp. 281–284.

50 J. Oh, M. Shin, J. Lee, J. Ahn, H. Baik and U. Jeong, *ACS. Appl Mater. Interfaces.*, 2014, **6**, 6954–6961.

Table of Contents